EFDA–JET–PR(13)51

M. Maslov, M.N.A. Beurskens, M Kempenaars, J. Flanagan
and JET EFDA contributors

Status of the JET LIDAR Thomson Scattering Diagnostic

Status of the JET LIDAR Thomson Scattering Diagnostic

M. Maslov, M.N.A. Beurskens, M Kempenaars, J. Flanagan
and JET EFDA contributors*

JET-EFDA, Culham Science Centre, OX14 3DB, Abingdon, UK

EURATOM-CCFE Fusion Association, Culham Science Centre, OX14 3DB, Abingdon, OXON, UK
** See annex of F. Romanelli et al, "Overview of JET Results",*
(24th IAEA Fusion Energy Conference, San Diego, USA (2012)).

Preprint of Paper to be submitted for publication in Proceedings of the
16th International Symposium on Laser Aided Plasma Diagnostics, Madison (Wi), USA
22nd September - 26th September 2013

ABSTRACT

The LIDAR Thomson scattering concept was proposed in 1983 and then implemented for the first time on JET tokamak in 1987. A number of modifications were performed and published in 1995, but since then no major changes were implemented for almost 15 years. In 2010 a refurbishment of the diagnostic has commenced, with as main goals to improve its performance and to test the potential of the new detectors which are considered as candidates for ITER. As a follow up during the subsequent years a wide range of activities was performed aiming to increase the diagnostic light throughput, improvement of signal to noise ratio and amendment of the calibration procedures. Previously used MA-2 detectors were replaced by fast GaAsP ones with much higher average QE. After all the changes implemented, a significant improvement of the measured data was achieved. Statistical errors of measured temperature and density were reduced by a factor of 2 or more, depending on plasma conditions, and comfortably surpassed the values requested for ITER Core Thomson Scattering (10% for T_e and 5% for n_e). Excellent agreement with other diagnostics (conventional High Resolution Thomson Scattering, ECE, Reflectometer) was achieved over a wide range of plasma conditions. It was demonstrated that together with long term reliability and modest access port requirements, LIDAR can provide measurements of a quality similar to a conventional imaging Thomson Scattering instrument.

1. INTRODUCTION

LIDAR Thomson Scattering was implemented successfully on JET more than 25 years ago [1,2] demonstrating the advantages of the LIDAR concept: 180 degrees scattering requires only one access port to plasma, light collection optics does not have to be a high resolution imaging optics, does not require precision alignment and is well suited for hazardeous environment where routine access might be difficult. The spatial resolution is limited by the laser pulse length and detector response time and can be optimized to ~7cm which leads to a spatial resolution of >8% of the minor radius for JET. For larger devices such as ITER this scales to >4% of the minor radius without the need for increasing the number of detectors. Because of these particular advantages, LIDAR was initially chosen as a profile diagnostic on JET and is considered as a candidate for the core plasma Thomson scattering diagnostic in ITER.

The latest publication on developments of the core LIDAR diagnostic on JET was released in 1995 [3]. Since then and until very recently, the diagnostic was running without any significant modifications. Recognizing that the produced data quality is far behind of the data produced by other more modern diagnostics (radiometer ECE, conventional high resolution TS) an extensive refurbishment was initiated in 2010 with the main goal to improve the quality of the measurements.

In this paper, description of the LIDAR diagnostic on JET will be given, with a special attention to details which represent the key differences between LIDAR and conventional TS design and which were not adequately highlighted in previous publications. Experience of using fast GaAsP detectors will be described, and examples of the measurements with achieved performance will be given, together with comparison with other diagnostics currently implemented on JET.

2. SCATTERING GEOMETRY AND COLLECTION OPTICS LAY-OUT.

2.1 OPTICS NEAR TOKAMAK

The layout of the LIDAR Thomson Scattering on JET is shown on figure 1. As one can see, all the major components of the diagnostic are located outside of the biological shield (2.5-3m of concrete), whilst only few light collection mirrors are placed near the tokamak. A short laser pulse is generated by a ruby mode-locked laser (694nm, ~300ps, ~1 Joule per pulse, 4Hz) and launched through an 8cm wide penetration tube towards a 45° mirror in the Torus Hall almost 20 metres below, and then horizontally directed into the JET plasma. Light scattered by plasma is collected via 6 different vacuum windows with d(iameter) = 0.16m located at the end of the JET pumping chamber ~4.4m away from plasma core. For each of the windows, a separate spherical mirror is collecting the scatter light and focusing into a small Newtonian mirror, which reflects the light down towards another 6 spherical mirrors which in turn focus the light into a biological shield penetration, d = 0.25m l = 2.5m.

Figure 2 shows calculated solid angle as if the scattered light was vignetted solely by the vacuum windows or by the collection mirrors. As one can see, in any plasma location the vacuum windows should be the stop aperture. Nonetheless, the real light throughput as measured during Raman scattering calibration is significantly more limited. The strong vignetting is imposed by the narrow penetration through the concrete ceiling of JET biological shield, thus limiting the radial extent of JET LIDAR profiles. The best light throughput point position can be controlled by adjusting the vertical collection mirrors and currently is set to ~3.5m in order to confidently cover the Low Field side part of plasma ~3.0-3.8m. The High Field side of the profiles is measured with much lower signal to noise ratio, and data for the innermost part may be missing.

Overall, maintenance of the collection optics is quite simple. There are in fact 6 independent light collection assemblies, 2 spherical mirrors in each and all sharing single small plane mirror. This is done to maintain high enough total collection solid angle, since the distance between the mirrors and JET plasma is very large (~8 metres, higher than foreseen for ITER). In order to maintain alignment stability, all 12 spherical mirrors are mounted on a concrete tower which is separate from the machine. Approximately once a year the whole assembly has to be removed to allow remote handling access to the interior of JET vessel and then put back, but no re-alignment of mirrors is normally required after the reposition.

2.2 IMPLICATIONS ON STRAY LIGHT.

Due to extremely low Thomson scattering cross section (~0.7×10^{-24}cm^2), every single TS instrument has to deal with combination of very low detectable signal on a background of a very bright diffused laser light. Dealing with LIDAR stray light is somewhat different from the conventional TS case. The fast detection system can discriminate various reflections of the short powerful laser pulse as a series of temporally separated spikes. The strongest splash of light is observed as the laser hits the inner wall of the vacuum vessel. Since the impact point of the laser is in direct line of sight of the powerful light collection optics, the so-called “backwall pulse” is traveling straight into the

spectrometer and even has a potential of damaging sensitive detectors or acquisition electronics. In the previous setup with MA-2 detectors, an overvoltage protection circuit was used. Presently, GaAsP detectors are connected directly to the digitizers (Tektronix TVS645) and no damage was developed so far.

The powerful backwall spike is coming *after* the useful signal and can be easily separated from it, as long as the probing laser does not produce pre-pulses. Pre-pulse rejection of the laser implemented on JET is of an order 10^{-6} and never caused problem with the stray light rejection arrangements currently implemented in the spectrometer.

Second highest spike is being seen at the time when the laser pulse is going through the input vacuum window. This is happening before the main signal and would have saturated previously used multi-alkali MA-2 detectors, therefore fast gating of these detectors was necessary. Large distance between the vacuum windows and plasma on JET (~3.5m) serves as a delay between this stray light spike and useful signal. That creates a large enough time gap to switch the detectors on and measure the passive background light before the laser pulse reaches plasma. Currently used GaAsP detectors are also gated in the same way, although no tests were performed to estimate the impact of that stray light on the detectors linearity and it is unknown if such gating is still compulsory.

In the proposed ITER LIDAR design [4], the backwall and the input aperture are the only two sources of stray light. However in the JET instrument an additional source is found in the laser beam penetration into the Torus Hall which is just a few centimeters away from the TS light penetration. Stray light from this penetration is in a field of view of the light collection optics in the Torus Hall, which is collecting it and sending back up into the spectrometer. Multiple reflections between the vacuum windows and collection mirrors produce the time delay so that certain reflections are mixing up with the useful TS signal. Required stray light rejection in the spectral channels closest to the laser line (~10^{-4} – 10^{-6}) is mainly dictated by intensity of the spurious reflections which must be suppressed.

3. JET LIDAR SPECTROMETER.

3.1 GENERAL SCHEME

The current spectrometer lay-out is slightly different from what is described in [2] and a schematic is show on figure 3.

A lens L1 at the end of the neutron shield penetration (below the left metal bucket in figure 2) is imaging 6 horizontal mirrors in the Torus Hall to a field lens marked as L2, which in turn is being relayed to the first shortpass interference filter F1 with cut-off wavelength just below the ruby laser line. It reflects the ruby light and all TS light of higher wavelength branch into the 1st detector, which has 2 stray light filters in front providing ~10^{-6} rejection. Lower wavelength branch is relayed to the filter stack F2, which consists of two wedges coated on both sides as shortpass filters with different cut-offs (described in [2] but were installed in the spectrometer only in 2013). Light is reflected into channels 2–5 depending on wavelength, and the shortest wavelength (<500nm) are going through to the spectral channel 6.

Physical size of the spectrometer is around 4m × 2m × 1m excluding the 2 metal columns and first 2 lenses. Diameter of all major components is 15cm and about 1m distance between the subsequent imaging planes gives a theoretical maximum etendue of the spectrometer around 500 sr*mm^2, but in reality only a small fraction of that is being used. Biological shield penetration is narrower than it was planned at times when the spectrometer was designed, therefore the maximum light spot size at the pupil is almost twice as small as the lens size, which decreases the actual etendue by about factor of 4: ~125sr*mm^2. Even that number is overestimated, since the image which is being relayed to all the interference filters and detectors is not a uniform circle (see figure 4) with quite considerable areas not illuminated (i.e. not used). Etendue of the actually collected light is about 40sr*mm^2, i.e. 10 times smaller than the spectrometer could have handled.

Despite the apparent inefficiency in using the spectrometers optical power, relaying the 6-spot image to the filters and detectors serves an important purpose. Shortpass filters with such spectral range of transmission/rejection require many dielectric layers to be coated. Making such a coating totally uniform over a large area is difficult if not impossible. Spectral transmission of each filter used on JET *is indeed different* at different areas, therefore the actual average transmission depends on the illumination of its surface. But since an image of the tokamak windows and not the plasma itself is being relayed – the scattered light footprint on each surface remains the same for each radial location along the collection path, and hence the spectral response of the spectrometer remains homogeneous and can be easily calibrated.

Another important aspect of such spectrometer design is stray light rejection. The large backwall stray light spike is at least 10^9 times stronger than the main signal (as measured on JET by stacking neutral density filters) and to completely neglect it one would require ~10^{-11} rejection. If only one-millionth part of it by diffuse scattering will come to a detector few nanoseconds earlier via some short-cut route to mix up with scattered light, we would need to add extra 10^{-5} ruby light rejection to that channel. For a high etendue spectrometer this is another expensive component to add to each spectral channel and leads to extra light losses. JET LIDAR spectrometer is designed in a way which excludes any possible shortcut routes for the backwall stray light flash. Only two spectral channels (1+2) are using extra stray light rejection filters, others can function unprotected.

3.2 DETECTORS

Fast GaAsP detectors (Hamamatsu 3809U-73A) with sensitive area d~11mm where previously used for the edge LIDAR on JET [5,6]. Operation of that diagnostic was suspended in 2009 therefore detectors become available for the core LIDAR. The main challenge for replacement of the previous MA-2 detectors by the new ones was to adapt the image size to a smaller area (from 18mm to 11mm), which required going from f/1.2 imaging to ~f/0.75. This was achieved by using a strong meniscus lens in addition to the existing doublet (see figure 5). The lens had to be made of a glass with high refractive index, therefore N-SF6 was chosen (n~1.8). Note that the glass spectral transmission is limited to λ>400nm.

3.3 NOTES ON CALIBRATION.

Spectral calibration of the instrument is described in [2] and hasn't changed much. Additional procedure was introduced to take into account non-uniformity of the interference filters and detectors response. Each of the six apertures of the spectrometer is now illuminated independently and the final relative sensitivity of spectral channels is calculated as a combination of them. On figure 6 one can see the results of 6 calibrations and observe the differences between them.

Calibration of the density profile shape, i.e. the light throughput at different radial position is done using Raman scattering from nitrogen at ~400mbar pressure. Highly doped Ruby crystal [7] is used to neglect the parasitic laser light, while the interference filters used during normal plasma measurements are removed. The Ruby filter is composed of 64 small cubes 5x5x15mm glued to each other, therefore only the light which incidents almost normally to its surface is propagating through undisturbed. Filter also has a relatively small total aperture (d~40mm), which is not enough to cover the whole input of the spectrometer. The only way to effectively use it for calibration is to install it just after the L2 lens (see figure 3) where the angles variation is the lowest and the image is composed of 6 independent light spots about ~35mm diameter, which can be covered by the ruby filter separately. That way calibration has to be done 6 times and final result will be a combination of them.

Only shape of measured density profile is calibrated via Raman scattering, absolute value of density is calculated by cross-calibration with far-infrared interferometer measurements. This is done once at the beginning of each experimental campaign and remains accurate within few %s for months.

Measuring Raman scattered light is also possible in a normal setup, with only interference filters rejecting the laser stray light. Comparison between the two types of calibration is shown on figure 7. As one can see the results are different – measurement with interference filters is wrong. This is caused by sensitivity of the interference filters cut-off wavelength to the angle of incidence, which is different for scattered light coming from different radial coordinate inside JET. It means that the Raman calibration without ruby filter is not possible to perform accurately in the current JET LIDAR setup. To minimize the error one would need to reduce the incidence angles variations on the filters thus increasing the filters diameter even further, implications of that for the ITER LIDAR design are discussed in [8]. Note that the property of passive absorption of the laser wavelength by the laser crystal material is unique to 3-level systems such as Ruby. If Nd:YAG is used as a laser source then the method implemented on JET for the stray light suppression will not work.

4. SUMMARY OF RECENT MODIFICATIONS TO THE DIAGNOSTIC.

In order to achieve better accuracy of the measurements, a number of changes were made to the JET LIDAR diagnostic. Review of the standard calibration scheme [9,10] has lead to the introduction of new procedures (e.g. calibration of 6 different apertures individually).

Vacuum windows spectral transmission is being measured regular since 2005 (figure 8). Thin coatings on the windows has a chromatic effect (transmission at blue is worse than at red) which

produces ~5% bias of the measured Te if not taken into account.

Lens L2 (figure 3) was initially an achromat used to operate a single point Thomson Scattering diagnostic in parallel with LIDAR while the latter was commissioned. This was actually 2 lenses made of BK7 and SF2 glass bonded to each other, with outer surfaces missing AR coating. Since the single point TS was decommissioned long ago, the achromat has recently been replaced by a simple BK7 plano-convex lens with a similar focal distance and AR coated for 400-800nm, which recovered about 8% signal in channels 1-5 and about twice as much in channel 6 due to poorer transmission of SF2 in that wavelength region.

A new collection optics alignment scheme was developed and used to improve the light collection efficiency. Implementation of the scheme during the 2009-2011 JET shutdown has shown that virtually no adjustment was required for 5 out of 6 collection sub-systems, but the last one was completely lost for unknown reason for unknown period of time (first was noticed in 2007). Alignment was restored therefore $1/6^{th}$ of the total collected light was recovered.

Four plane plate filters at stack F2 (figure 3) [2] were replaced by wedges coated on both sides. Plane filters didn't have an AR coating on their back side which created unnecessary light losses especially for high temperature channels (for example to reach spectral channel 5, scattered light had to pass the other filters five times: 2-3-4-3-2)

GaAsP detectors were installed as described in section 3.2, with improved effective QE especially at 600-800nm where previous MA-2 detectors are very inefficient.

High aperture, high transmission (~85-90%) nanowire polarizer was installed in the system - in the past no polarization filtering was used. Factor of 2 reduction of plasma background light had a specially strong positive impact for high-Te measurements in H-mode plasma, where beryllium spectral lines are overwhelming spectral channels 5 and 6 (400-550nm). This problem was significantly enhanced after installation of the beryllium/tungsten ITER-like metal wall on JET [11], due to increase of Be concentration in plasma and possibly enhancing of observed background light due to reflections from the metal wall inside the new vessel.

5. OVERVIEW OF THE PRODUCED MEASUREMENTS AFTER THE UPGRADE.

In figures 9-11 one can find examples of the most recent LIDAR measurements in different plasma conditions (from very small to very large stored energies) together with estimated relative errors. Displayed uncertainties of the measurements are assuming only statistical errors and calculated with [12] using real signal to noise ratios in all spectral channels. Statistical error bars are designating a +/- 33% confidence interval. One can see that quality of the measurement is varying at different radial coordinates, since light collection efficiency is changing as a function of radius (figure 2) and accuracy of measurement at lower temperatures (<1keV) is reduced due to the stray light suppression requirements in the spectrometer design (scattered light near 694nm is lost) and spectral channels near the laser line being too wide because of the interference filters design.

In plasmas with low n_e and T_e the errors in temperature are still below 10% and in density below 5% for most part of the plasma and become even better at R=3.0-3.5m where the diagnostic is most

efficient (figure 9).

In typical plasmas of interest (figures 10 and 11), errors are going below 5% and 3% respectively for T_e and n_e, which is far better than requested for the ITER LIDAR prototype (10% in Te and 5% density for $n_e>3*10^{19}$). Note that despite the more than a factor of two density increase between cases 2 and 3 (figures 10 and 11), quality of measurement is almost unchanged – this is due to enhancement of plasma background light which is growing together with density.

In table 1 a summary of the current and previous status of the measurements is shown. Note that the indicated improvement the in measurements accuracy only include statistical errors (signal to noise ratio) and does not take into account improvements in calibration.

Note that the spatial resolution remains the same and is currently limited by the slowest component - old digitizers which are still being used. Faster DAQ system is available on JET which would immediately allow us to achieve a resolution of ~7cm, but the implementation of the new system is currently pending a decision on the overvoltage protection.

Electron temperature on JET can be measured with three independent diagnostics: Electron Cyclotron Emission (ECE) [13], core LIDAR and conventional High Resolution Thomson Scattering (HRTS)[14]. Core density profile is in turn measured by LIDAR, HRTS and a microwave reflectometer [15]. Calibration of density is somewhat tricky, absolute value for both Thomson scattering diagnostics is cross-calibrated versus line integrate measurements of interferometer, which is considered accurate and reliable. Density profile shape of LIDAR is calibrated via Raman scattering as described above, HRTS density shape is in turn cross-calibrated to LIDAR in the core and reflectometer at the edge. Reflectometer is self-sufficient in terms of absolute density, but profile position is dependant on magnetic filed measurements and prone to be inaccurate, therefore has to be adjusted to the best match with interferometer edge measurements.

On Figure 12 one can find an example of all the mentioned diagnostic results plotted on the same equatorial plane coordinate axis – there is a very good agreement between all of them. Discrepancies between the diagnostics do occur as a result of a number of physical and technical reasons, which are outside of the scope of this paper. Although, these variations as observed during the experiments performed in 2011-2012 typically are within 5% margin.

CONCLUSIONS

JET LIDAR diagnostic produced its first results more than 25 years ago and is still operational. Despite a good record on JET, it remains unique in the fusion world as LIDAR requires a minimum size device in order to obtain a spatial resolution of <10% of the minor radius. The LIDAR concept becomes more attractive for bigger fusion devices with restricted access due to neutron radiation/ activation. In that case, simplicity of light collection optics and single port access to burning plasma, offered by LIDAR, becomes so compelling that it may outweigh the difficulties associated with laser and spectrometer/detectors design and development.

JET experience has shown that once the diagnostic is built, it is fairly easy to maintain and is capable to reliably produce data for many years. After the series of refurbishments done in 2011-2013,

the diagnostic is producing measurements of the highest quality ever, well surpassing the accuracy requested for the ITER Core Thomson scattering. The diagnostic is expected to stay operational in future JET experiments and produce measurements in the forth-coming full scale DT campaign.

ACKNOWLEDGMENTS

This work, part-funded by the European Communities under the contract of Association between EURATOM/CCFE, was carried out within the framework of the European Fusion Development Agreement. For further information on the contents of this paper please contact publications-officer@jet.efda.org.* The views and opinions expressed herein do not necessarily reflect those of the European Commission. This work was also part-funded by the RCUK Energy Programme under grant EP/I501045

REFERENCES

[1]. H. Salzmann, K. Hirsch, *Proposal for a time - of - flight Thomson backscattering technique for large fusion devices,* Review of Scientific Instruments **55**, 457 (1984)

[2]. H. Salzmann, J. Bundgaard, A. Gadd, C. Gowers, K.B. Hansen et al., *The LIDAR Thomson scattering diagnostic on JET*, Review of Scientific Instruments **59**, 1451 (1988).

[3]. C.W. Gowers, B.W. Brown, H. Fajemirokun, P. Nielsen et al., *Recent developments in LIDAR Thomson scattering measurements on JET*, Review of Scientific Instruments **66**, 471 (1995)

[4]. M. J. Walsh, M. Beurskens, P. G. Carolan, M. Gilbert, *Design challenges and analysis of the ITER core LIDAR Thomson scattering system*, Review of Scientific Instruments **77**, 10E525 (2006);

[5]. M. Kempenaars, J.C. Flanagan, L. Giudicotti, M.J. Walsh, M. Beurskens, I. Balboa, *Enhancement of the JET edge LIDAR Thomson scattering diagnostic with ultrafast detectors*, Rev. Sci. Instrum. **79**, 10E728 (2008)

[6]. L. Guidicotti, R. Pasqualotto, *Characterization of fast microchannel plate photomultipliers for the ITER core LIDAR Thomson scattering system*, 2012 JINST **7** C02037

[7]. C. Gowers, K. Hirsch, P. Nielsen, and H. Salzmann, *High rejection ruby filter for laser light scattering experiments*, Applied Optics, Vol. 27, Issue 17, pp. 3625-3629 (1988)

[8]. R. Scannell, M. Beurskens, M. Kempenaars et al, *Absolute calibration of LIDAR Thomson scattering systems by rotational Raman scattering*, Rev. Sci. Instrum. **81**, 045107 (2010)

[9]. K. Beausang, *The consistency of electron temperature measurements by Thomson scattering at the JET tokamak*, PhD thesis at the University College Cork (2011), Cork, Ireland.

[10]. J. Hawke et al, *Spectral Calibration of the JET Core LIDAR Thomson Scattering Diagnostic Using Ray Tracing*, submitted to Review of Scientific Instruments

[11]. G F Matthews et al., *JET ITER-like wall—overview and experimental programme*, Physica Scripta Volume 2011 T145

[12]. M Maslov et al., *Note: Statistical errors estimation for Thomson scattering diagnostics*, Review of Scientific Instruments **83**, 096106 (2012)

[13]. S. Schmuck, J. Fessey et al., *Electron cyclotron emission measurements on JET: Michelson interferometer, new absolute calibration, and determination of electron temperature*, Review of Scientific Instruments **83**, 125101 (2012)

[14]. R. Pasqualotto et al., *High resolution Thomson scattering for Joint European Torus (JET)*, Review of Scientific Instruments **75**, 3891 (2004)

[15]. A. Sirinelli et al., *Multiband reflectometry system for density profile measurement with high temporal resolution on JET tokamak*, Review of Scientific Instruments **81**, 10D939 (2010)

	Previous	**Current**
Repetition rate	4 Hz	4 Hz
Measurements area	-0.75<r/a<0.75	-0.4<r/a<0.95
Spatial resolution	12cm	12cm
Statistical error in Te(core) for ohmic plasma	>20%	<5%
Statistical error in Ne(core) for ohmic plasma	>10%	<3%
Statistical error in Te(core) for heated plasma	~10%	~3%
Statistical error in Ne(core) for heated plasma	~5%	~1.5%

Table 1: status of the measurements before and after the refurbishment.

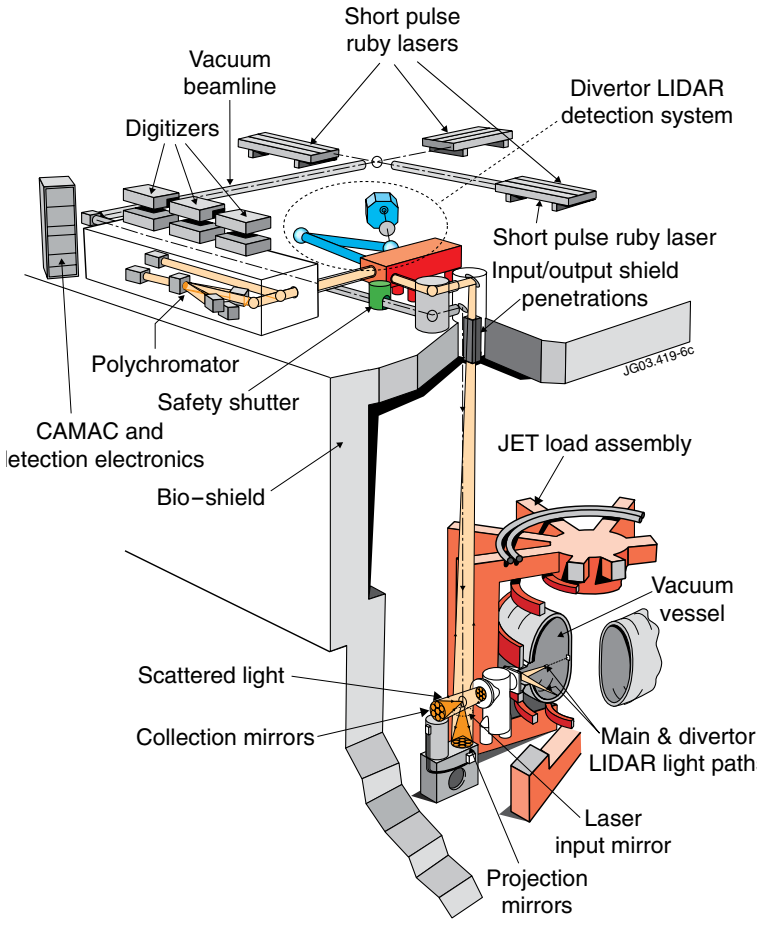

Figure 1: schematic of the JET LIDAR diagnostic.

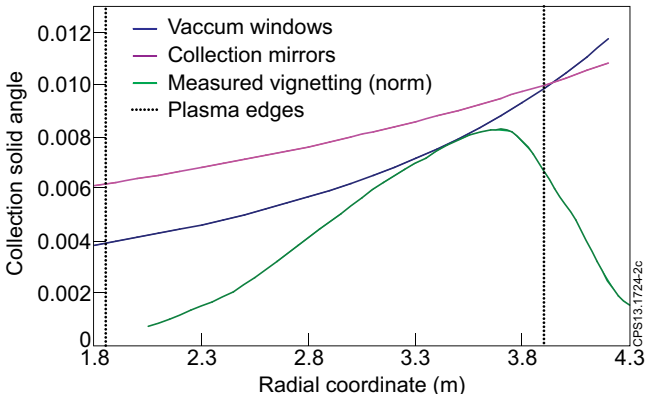

Figure 2: Light collection solid angle, seen by vacuum windows and collection mirrors, in comparison with real measured light throughput.

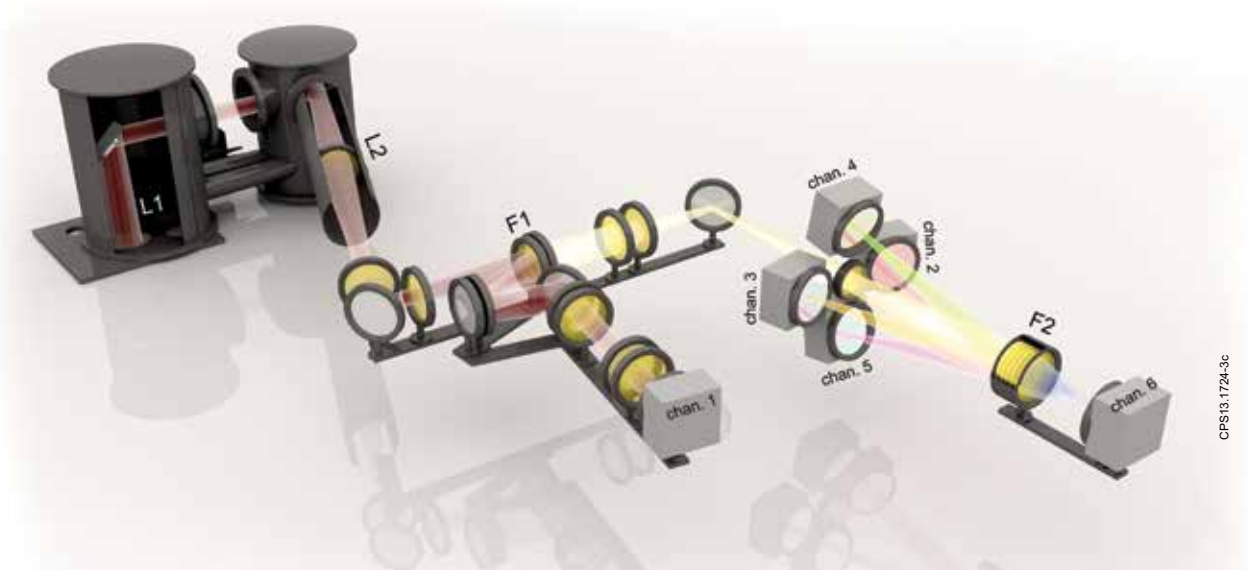

Figure 3: JET LIDAR spectrometer

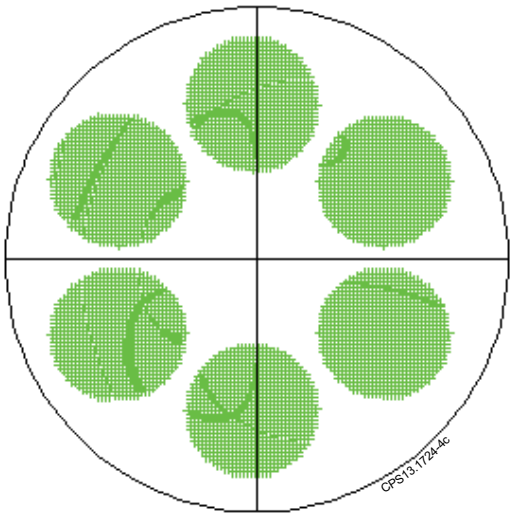

Figure 4: Image on the detector surface d = 11mm, as in the ray-tracing model.

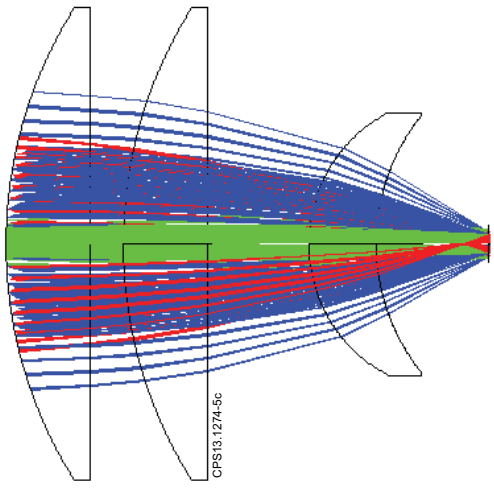

Figure 5: Ray-tracing model of image compression into d = 11mm detector surface. Light of different colours is coming from different positions in plasma.

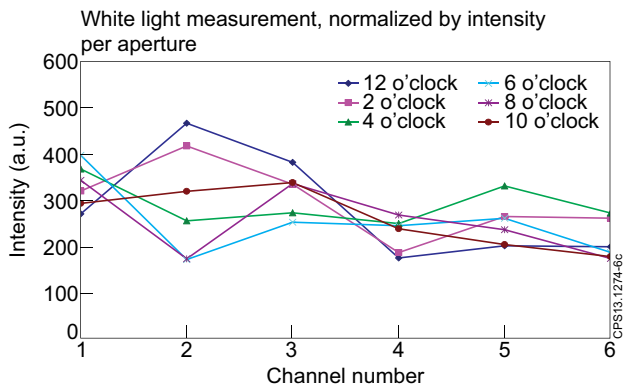

Figure 6: Variation of spectrometer response to calibrated white light source at each of the 6 input windows.

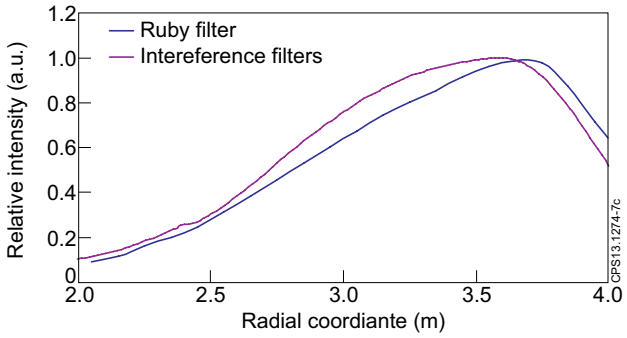

Figure 7: Results of the vignetting calibration, using ruby filter and dielectric interference filters for rejection of parasitic light. Both curves are normalized.

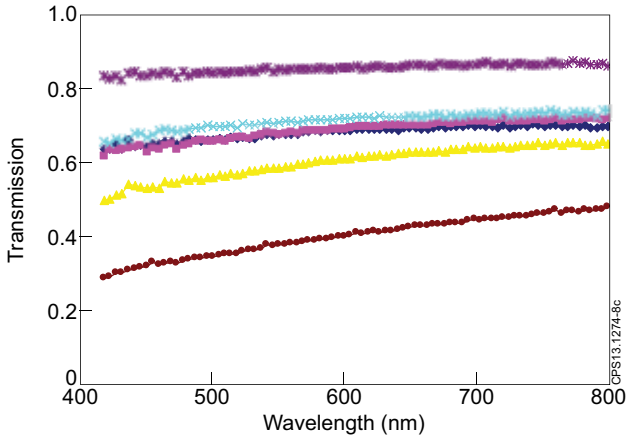

Figure 8: Spectral transmission of 6 LIDAR light collection window.

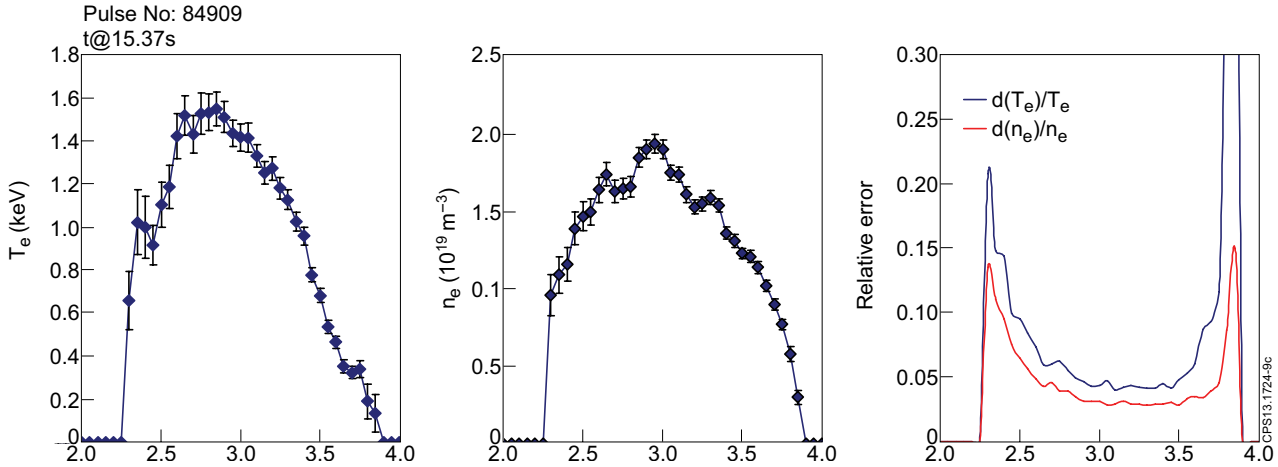

Figure 9: Example of LIDAR measurements, Ohmic low current plasma. Pulse No: 84909, t = 15.37s, I_p = 1.5MA, most unfavourable plasma for LIDAR.

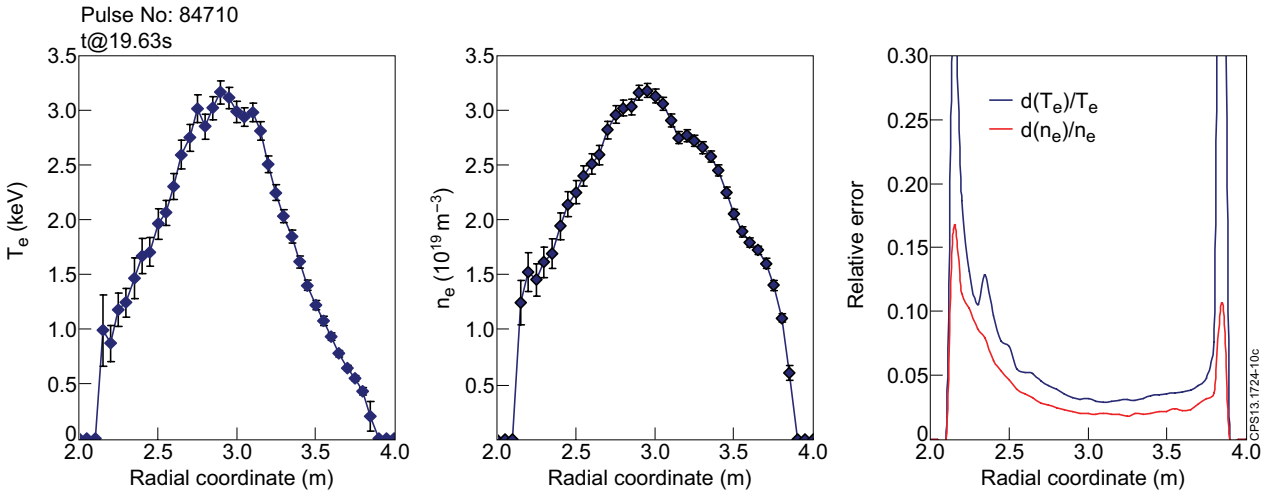

Figure 10: Example of LIDAR measurements, mild additional heating.
Pulse No: 84710, t = 19.63s P(NBI) = 3MW, I_p = 2.0MA.

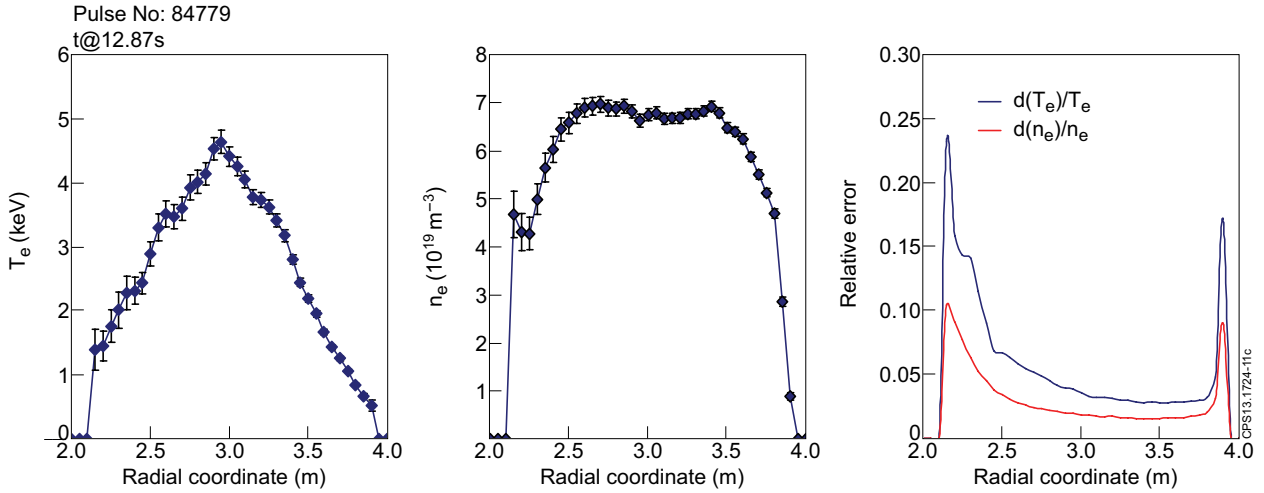

Figure 11: Example of LIDAR measurements, strong heating.
Pulse No: 84779, t = 12.87s, P(NBI) = 20MW, I_p = 3.0MA, solid baseline H-mode.

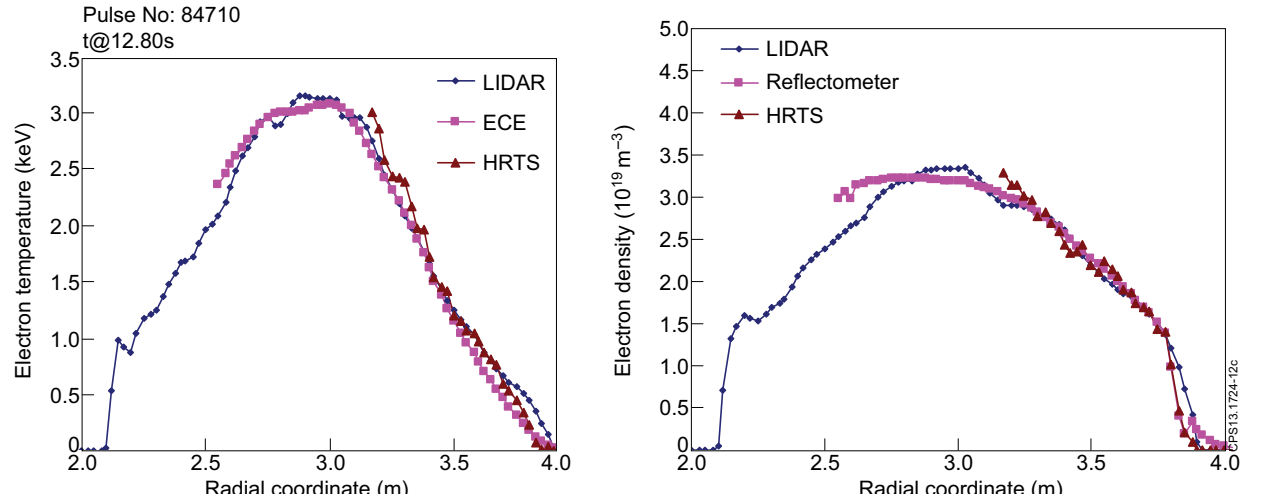

Figure 12: comparison of various temperature and density measurements available on JET.
Pulse No: 84710, t = 12.80-12.90s. All Te measurements are fully independently produced.